Experimental Investigation of a Wave-Piercing Trimaran on the Outrigger Configurations in terms of Seakeeping and Added Resistance

A. Askarian Khoob [1], S. Moghaddam Pour[1] and A. Feizi[2†]

[1] Department of Mechanical Engineering, Imam Khomeini Naval Academy, Nowshahr, Iran
[2] Department of Civil Engineering, Faculty of Engineering, University of Mohaghegh Ardabili, Ardabil, Iran

†Corresponding Author Email: a_feizi@uma.ac.ir

ABSTRACT

The outrigger symmetry of a trimaran is believed to significantly affect its hydrodynamic functioning. The present study was conducted to investigate the added resistance responses and experimental vertical motion of a wave-piercing trimaran in regular head waves. A series of experiments have been carried out in the National Iranian Marine Laboratory (NIMALA) towing tank to determine the effect of side hulls symmetry on the heave and pitch motions and added resistance. The models were tested over a range of wave frequencies and Froude numbers using both symmetric and asymmetric outriggers. According to the results, the symmetric side hull form based on heave motion, the outboard form in terms of pitch motion and added resistance have better performances among these three kinds of side hull forms. Furthermore, there are local maximum and minimum points on the ship motion response curves due to heave and pitch coupling in their respective frequencies.

NOMENCLATURE

B	breadth of the main hull	Z	heave amplitude
C_z	non-dimensional heave amplitude	θ	pitch amplitude
C_θ	non-dimensional pitch amplitude	σ_{AW}	added resistance coefficient in non-dimensional form
F_r	Froude number		
g	acceleration of gravity	ξ	amplitude
k	incident wave number	ρ	fluid concentration
L	length of the main hull		
R_{AW}	added resistance		
R	longitudinal positions of the side hulls transoms towards the main hull transom	ω	incidence wave frequency
		ω_e	encounter wave frequency

1. INTRODUCTION

Trimarans, have attracted a growing interest for designers and shipyards for car/passenger ferry and naval applications over the last decade. Trimaran is composed of a long slender main hull, two very fine side hulls, and two cross deck structure joining the three hulls together. Owing to its specific structure configuration, trimaran can offer several advantages over an equivalent catamaran and monohull, including superior seakeeping ability in waves, better powering performance at high speed, and high survivability in damaged condition, better transverse stability, and a large open deck area. It is also worth mentioning that, unlike the monohull, the trimaran concept could be designed in various ways and allows the designer a wide range of choices on hull form variables to achieve desirable hydrodynamic performance. The predominant parameters are seen to be the side hull symmetry, displacement ratio, the water plane areas of the three hulls, and the relative positions of outriggers and main hull. To comprehensively understand the effects of these variables on trimaran performance, further extensive investigations are certainly required.

Armstrong (2006) presented the measurements conducted on a fast ferry trimaran during the full-scale trials. Furthermore, a comparison was made between the trimaran and the equivalent catamaran. The results have demonstrated reduced roll and pitch motion and a 50% reduction in crew and passenger seasick for the trimaran. Fang *et al.* (2006) developed a 3D FSI model to study the impact of outriggers position on the motion of a trimaran in regular waves. Their results showed that the larger clearance and smaller stagger of side hulls are generally advantageous for the trimaran ship design. Davis and Holloway (2007) computed the motions of trimarans and catamarans employing a time domain seakeeping method. They found that the roll motion of a trimaran increases with the reduction in the buoyancy of side hulls. Hebblewhite *et al.* (2007) experimentally studied the influence of the stagger position of the side hulls on the seakeeping behaviour of a representative trimaran. They conducted seakeeping tests for four different stagger positions. Their studies revealed that with aftward shifts in the outrigger position, the heave and pitch motion of the trimaran decreased. Wu *et al.* (2011) computed the ship motion and added resistance for a high-speed trimaran using the CFD method. They provided a numerical tool for the study of the seakeeping performance of high-speed trimarans. Pérez Fernández (2012) carried out the numerical frequency and time-domain research on the seakeeping performance of a fast ferry trimaran for operations in the Mediterranean Sea. Pavkov and Morabito (2014) conducted an experimental investigation into the resistance, heave, and trim of two trimarans ship in shallow and deep water. Their result demonstrated a strong increase in the resistance and sinkage near the critical speed.

Akbari *et al.* (2014) experimentally investigated the dynamic behaviour of a trimaran in terms of heave and pitch motions of the wave piercing trimaran in regular head waves at different vessel speeds. Jiang *et al.* (2016) performed a combined numerical and experimental study on the hydrodynamic behaviour of a tunnel and its influence on the hull performance of a planning trimaran. Deng *et al.* (2016) reported the influences of hull form slenderness on the global hull girder loads and seakeeping performance of trimaran using the WASIM code based on a time-domain 3D Rankine source method. Their result implied that the slenderer hull contributes to a sharp increase in the shear force and total longitudinal bending moment, but leads to better seakeeping performance. Poundra *et al.* (2017) numerically worked on optimizing a trimaran yacht equipped with an axe bow. They concentrated on the analysis of seakeeping and resistance utilizing ANSYS Fluent code for resistance analysis and seakeeper from Maxsurf for seakeeping analysis. Wang *et al.* (2018) considered the optimization of the trimaran model applying numerical and experimental methods. They provided the optimal outrigger layout of a trimaran with the minimum roll, pitch, and heave motion. Jiao *et al.* (2019) conducted comprehensive experimental and numerical studies to examine the wave-induced load and motion responses of a trimaran ship with large-scale model sea trial and small-scale model in

towing tank. Their results provided a practical reference for the fast measurement of ship wave-induced load and motion responses in short-crested waves based on the long-crested wave responses. Combining the PID autopilot model and time-domain retardation function, Chen *et al.* (2019) developed a 3D nonlinear hydroelastic method to assess the responses of the wave-induced load and the motion of a trimaran with flexible hulls in oblique irregular waves. Furthermore, they performed the experimental tests with a segmented trimaran model. Their findings confirmed that their model is accurate and reliable for the prediction of nonlinear hydroelastic responses of ships in oblique irregular waves. Li and Li (2019) carried out experimental and numerical studies into the interference effect of trimaran equipped with and without a T-foil near the bow on the longitudinal motion characteristics. They demonstrated that the longitudinal motion response values decrease greatly with the use of T-foil. A viscous method based on RANS was employed by Deng *et al.* (2019) to study the added resistance and motion response of a trimaran in regular head waves and the resistance in calm water. Applying a hybrid method, called the QaleFOAM, Gong *et al.* (2020) investigated the added resistance of a trimaran ship and seakeeping performance in oblique waves. Their results demonstrated that the trimaran variation trend of responses was crucially impacted by the wave heading and wave steepness, which is different from the traditional mono-hull ships. Nowruzi *et al.* (2020a) performed a CFD simulation of trimaran to evaluate heave and pitch motion responses in regular head waves. The CFD results were compared to a set of model test results, and the results suggested that CFD offers a reliable method to predict pitch and heave motions of trimarans in regular head waves. Tang *et al.* (2020a) conducted a series of model tests to calculate wave-induced load and motion response of trimaran in the small heeling angles under regular and irregular waves. Moreover, numerical simulations were applied in their research according to 3D potential flow theory for the investigation of the motion and load characteristics of trimmers. Their results indicated that in small heeling conditions, the roller and pitch motion of the trimaran obviously increases although the heave motion is lighter. Nowruzi *et al.* (2020b) studied the effect of side hull position on the seakeeping performance and added resistance of a trimaran in oblique waves. They demonstrated that arranging the side hulls according to the centre hull stern decreases the added resistance by up to 20%, whereas, it increases the roll motions. Tang *et al.* (2020b) developed a new kind of nonlinear predicting method based on the 3D time-domain Rankine-Green matching method for studying the wave-induced load and motion responses of a trimaran ship. Their results proved the suitability of this method for the structural strength assessment and detailed design of trimaran with small bulbous bow and side hull stern, particularly at relatively high sailing speeds.

As could be seen, the majority of previous studies have focused on the influence of stagger and separation position of side hulls on the hydrodynamic performance of trimaran. The reliable

data concerning the outrigger forms and their effects on the dynamic behaviour of trimarans is restricted. Therefore, the present study aimed to comparatively investigate the heave and pitch motion constituents on top of added resistance of a trimaran with three alternative side hulls, including symmetric, asymmetric outboard, and asymmetric inboard forms. Three different configurations of symmetric and asymmetric models were experimentally tested at zero and forward speeds at various wave frequencies and wave heights in regular head waves.

2. TOWING-TANK TESTS

2.1 Physical description of the model

A 1:80 scale model of a trimaran was built up to main deck level according to ITTC 7.5-01-01-01 procedure with polyethylene material with the capability of proper machining, superior resistance to water absorption, and excellent impact-resistant performance. Table 1 represents the main properties of the full and model scales of the trimaran. The model had a quite slender (L/B = 12.96) main hull with a wave-piercing bow and reversed flare arrangement profile, which has several significant hydrodynamic and efficiency characteristics. Two side hulls were considered with a Wigley hull form in symmetric shape, and one side Wigley and another side were flat in asymmetric form. Three individual hulls were linked using a transverse rigid aluminum tube, which allowed easy change of separation positions of the side hulls and reconfiguration of the model. A longitudinal aluminum beam was designed and fabricated for the change of stagger position of the side hulls. Figure 1 depicts the model and lines drawn of the trimaran hulls.

Table 1 Main properties of the prototype trimaran and its scaled model

Particular [unit]	Full scale	Model scale
Length overall [m]	124.38	1.555
Length on waterline [m]	123.24	1.541
Length between perpendiculars [m]	120.10	1.501
Beam overall [m]	21.78	0.272
Beam on waterline [m]	9.612	0.121
Depth [m]	11.78	0.147
Draft [m]	4.38	0.055
Length of side hull [m]	36.00	0.450
Beam of the side hull [m]	2.362	0.030
Depth of the side hull [m]	8.136	0.102
Draft of the side hull [m]	2.72	0.034
Displacement [ton]	2249	0.0044

2.2 Experimental setup

The model tests were performed in the National Iranian Marine Laboratory (NIMALA) towing tank facilities. It was 400 m long, 6 m wide, and 4 m deep.
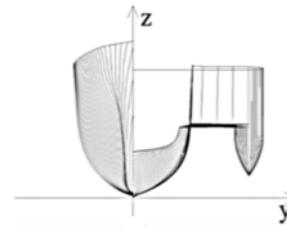
(a)

(b)

**Fig. 1. (a): Trimaran model and (b): Lines drawn of the central hull and side hull.**

The towing carriage is a manned vehicle with dimensions of 7 * 7.6 metres with two velocity ranges. Its low and top motor velocities are in the range of 0.5 to 5 m/s and 4.5 to 19 m/s, respectively. This towing tank, as the most efficient and largest country reference, was established in 2013 to carry out all design and engineering tests for surface ships and submarines. NIMALA joined in Towing Tank Conference (ITTC) in 2017. NIMALA towing tank facility is depicted in Fig. 2. The towing carriage includes a dynamometer for resistance measurement and two potentiometers to record the bow and astern motions of the model during the tests (Fig. 3). The model was connected to the dynamometer via a towing post with a heaving road and a hinged mechanism, and two trim guides and potentiometers from the bow and astern. Therefore, for full head seas, the model was free to heave, pitch, and roll motions while being constrained for surge, sway, and yaw motions. The towing post was connected to the model at the intersection of the propeller shaft line with the vertical centres of gravity to minimize the artificial trim effects.
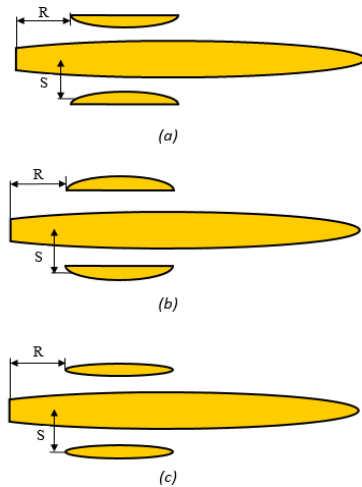

Fig. 2. A view of NIMALA towing tank with a carriage.

2.3 Test Matrix

The testing was carried out in two lateral (separation) positions and two longitudinal (stagger) positions of
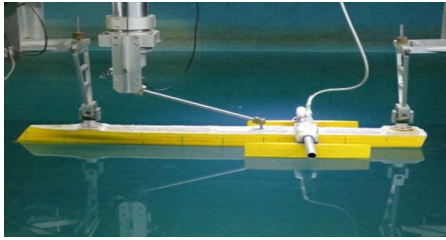
Fig. 3. Experimental set up of the model.

Fig. 4. Stagger and separation definition. (a) Asymmetric Inboard; (b) Asymmetric Outboard; (c) Symmetric.

side hulls utilizing both the symmetric and asymmetric forms. Following the completion of the series of experiments with asymmetric outboard side hulls, two side hulls were reversed so that their flat side would be placed outwards. The experiments were repeated for asymmetric inboard side hulls. Figure 4 illustrates the definition of the longitudinal and lateral spacing between the main and the side hulls. The position of the side hulls was notified as separation ratio (S/L) and stagger ratio (R/L), in which S shows the distance between the main hull centreline and the side hulls centreline, and R is the longitudinal positions of the side hulls transoms towards the main hull transom. L is the length of the main hull at the waterline. For the same separation distances, all the three side hull forms possessed the same maximum overall beam and the same minimum tunnel width. In addition, the ship model moment of inertia apparatus equipment was used for the determination of the pitch radii of gyration. Table 2 shows various configurations of the trimaran's lateral and longitudinal spacing and pitch radius of gyration. The model tests were conducted in regular head wave conditions. Seven regular type waves from 0.6 m to 2.4 m wavelength at 0.3 m increments were considered as incoming waves. The amplitudes of incident waves were 25 and 35 mm in the model scale. The model speeds were 0.0, 0.58, 1.155, and 1.73 m/s which is equivalent to the full scale speeds

0, 10, 20, and 30 knots (corresponding to Froude numbers of 0.0, 0.15, 0.30, and 0.45), respectively. The model-scale tests matrix is presented in Table 3. The model tests matrix involved two groups of experiments, including zero speed and forward speed. Zero speed tests were conducted with a carriage positioned in the middle of the tank. In the forward speed tests, the model was released from the docking station so that the generated waves reach the model within 75% of the length of the tank from the wave maker. In order to have enough accuracy in the tests, according to the ITTC 7.5-02-05-04 procedure, more than 75 incident waves hit the model. To avoid the occurrence and subsequent spurious measurement of results in the presence of any reflected waves and residual decaying, a waiting period between the respective tests of 45–60 minutes (depending on the wave amplitude and frequency) was allowed. The water surface was also visually controlled.

Table 2 Lateral and the longitudinal Position of side hulls and radius of gyration

Configuration	Stagger ratio	Separation ratio	Pitch radius of gyration
Asymmetric inboard	0.15	0.14	0.276
Asymmetric outboard	0.15	0.14	0.276
Symmetric	0.15	0.14	0.276

2.4 Data recording and analysis

For each test, the added resistance and motion amplitudes were continuously recorded for an elapsed period of 150 seconds at a sampling frequency of 100 Hz. Two potentiometers and dynamometers measured the resistance, bow, and astern motions of the model in the time domain mode. These data were translated based on the time

Table 3 Characteristics of the test program

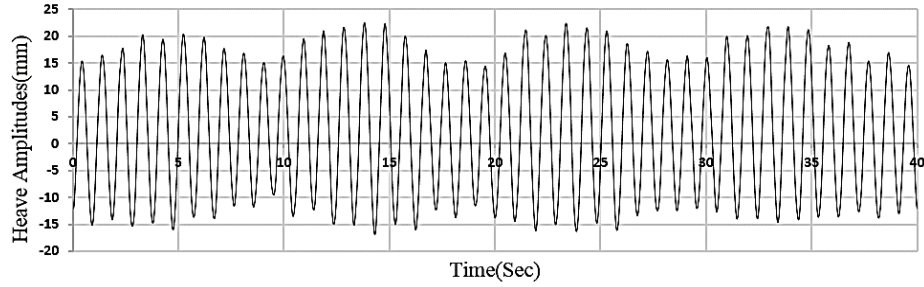| Froude Number	Amplitude ξ(mm)	Frequency ω (rad/s)	Hull Form
0 0.15 0.3 0.45	25 35	5.0638 5.4139 5.8468 6.4048 7.1608 8.2688 10.1277	Asymmetric Inboard
			Asymmetric Outboard
			Symmetric
2 (Amplitudes)*7 (Frequencies)*4 (Froude Numbers)*3 (Hull Form) = 168 runs			

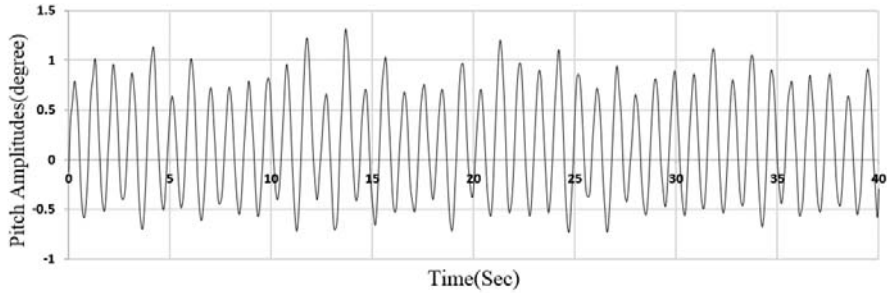**Fig. 5. Time history of heave motion with outboard asymmetric outrigger (F$_r$= 0.15, ζa=0.025 m, ω=5.0638 rad/sec).**

Fig. 6. Time history of pitch motion with outboard asymmetric outrigger (F$_r$= 0.15, ζa=0.025 m, ω=5.0638 rad/sec).

domain into the frequency domain using the Root Mean Square (RMS) method of data analysis.We developed a MATLAB code to calculate the RMS. The code initially introduces the recorded time series and trims the signal to a specific portion of the signals to be analyzed. The signal was detrended to remove high-frequency components, followed by the identification of absolute peaks. Figures 5 and 6 illustrate the time history of the heave and pitch motions responses in head sea conditions

The results obtained from the towing tank tests were changed to a non-dimensional form and noted as the response amplitude operator (RAO). The non-dimensional heave and pitch amplitudes were defined as follows (ITTC, 2017):

$$C_z = \frac{Z}{\xi_a} \quad (1)$$

$$C_\theta = \frac{\theta}{k\,\xi_a} \quad (2)$$

where Z is the heave amplitude, θ is the pitch amplitude, ξ_a shows the incident wave amplitude, and k represents the incident wave number, $\frac{2\pi}{\lambda}$. The added resistance coefficient in non-dimensional form was defined as follows (Deng *et al.* 2019):

$$\sigma_{AW} = \frac{R_{AW}}{\rho g \xi_a^{\,2} B^2 \big/ L} \quad (3)$$

where R_{AW} illustrates the added resistance, L and B are the length and breadth of the main hull, respectively, ρ is the fluid concentration, and g shows the acceleration of gravity.

The horizontal axes represent the non-dimensional encounter wave frequency$\omega_e \sqrt{\frac{L}{g}}$. ω$_e$ is given in Eq. (4):

$$\omega_e = \omega - \frac{\omega^2}{g} U \cos\beta \quad (4)$$

where ω illustrates the incidence wave frequency (rad/s), U is the model speed (m/s), and β is the wave heading angle (for head wave β = 180°).

3. RESULTS AND DISCUSSIONS

Based on the results of the experimental model test, the Response Amplitude Operators (RAO) of heave and pitch motions as well as resistance force were drawn for two different values of the wave amplitudes of 25 and 35 mm. The relationship between the heave motion and the non-dimensional encounter wave frequency for three different side hulls are presented in Figs. 7 and 8.

Figure 7 shows the comparison of heave RAO at the wave amplitude of 25 mm. As depicted in Fig. 7, the heave responses were linear versus wave frequencies for the non-dimensional encounter frequencies ranging from 2.01 to 2.54 at the zero speed model

(F_r=0), 2.4 to 2.8 at the model speed of 0.58 (F_r=0.15), and 2.73 to 3.28 at the model speed of 1.155 m/s (F_r=0.3). The responses revealed a nonlinear behaviour at the remaining frequencies. There was an unequivocal difference between their behaviour of responses at the model speed of 1.73 m/s (F_r=0.45), which was nonlinear versus wave frequencies at all the ranges of frequencies. It could be seen that the responses were sensitive to the model speed and the magnitudes of the responses decreased with the increase in the model speeds. Nevertheless, the plots contained some kinks (local minimum and maximum) in the responses at higher frequencies for the individual vessel speeds.

The plots of the heave motion responses at the zero speed (Fig. 7(a)) comprised mild single "kinks" at the non-dimensional encounter frequencies of 2.84 and 3.28 for the outboard and symmetric side hull forms, respectively. As shown in Fig. 7(b), at the model speed of 0.58 m/s (F_r=0.15), a single mild kink could be seen for the inboard and symmetric hull forms at a non-dimensional encounter frequency of 3.57 and for the outboard at non-dimensional frequency of 4.25. As the vessel speed increased to 1.155 m/s (F_r=0.3) and cruising speed of 1.73 m/s

(F_r=0.45), the responses for the models become very distinct in behaviour. At the speed of 1.155 m/s, outboard and inboard side hull responses contained double moderate kinks (Fig. 7(c)) at the non-dimensional encounter frequencies of 3.7 and 5.2 and at the speed of 1.73 m/s, they contained two big kinks (Fig. 7(d)) at the non-dimensional encounter frequencies of 4.26 and 5.15 while the peak magnitudes of these kinks were different.

Vessel motion responses are magnified at appropriate modes of natural frequencies, which could be shown both in theory as well as in practice. In addition to these frequencies, it is theoretically proven and occasionally confirmed by the model tests with multihull vessels that there are other sets of critical frequencies called "interference" or "standing wave" frequencies. In these frequencies, the vessel motions may be affected particularly in the beam seas at zero speed. These frequencies may be more effective on twin-hulls, like SWATH ship with long vertical-sided struts, where the development of the standing wave can be easier. The standing waves could be formed in transverse as well as in longitudinal direction (Atlar *et al.* 1985).
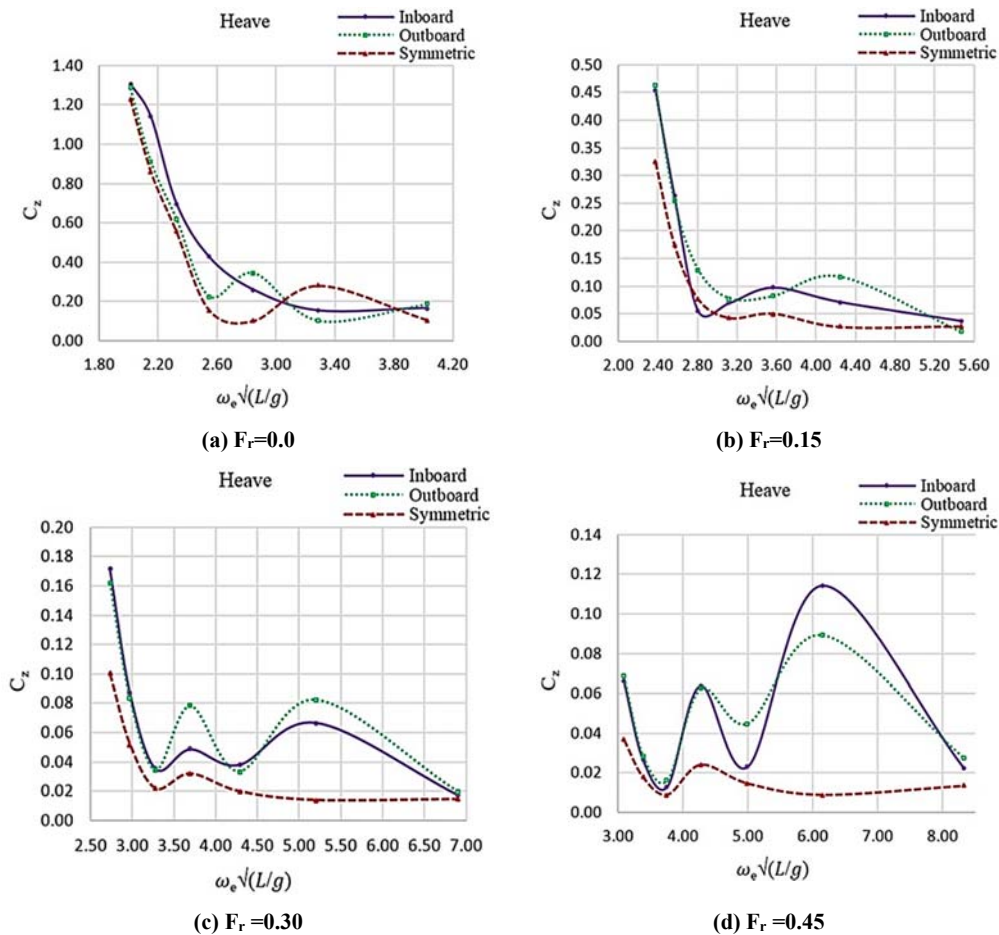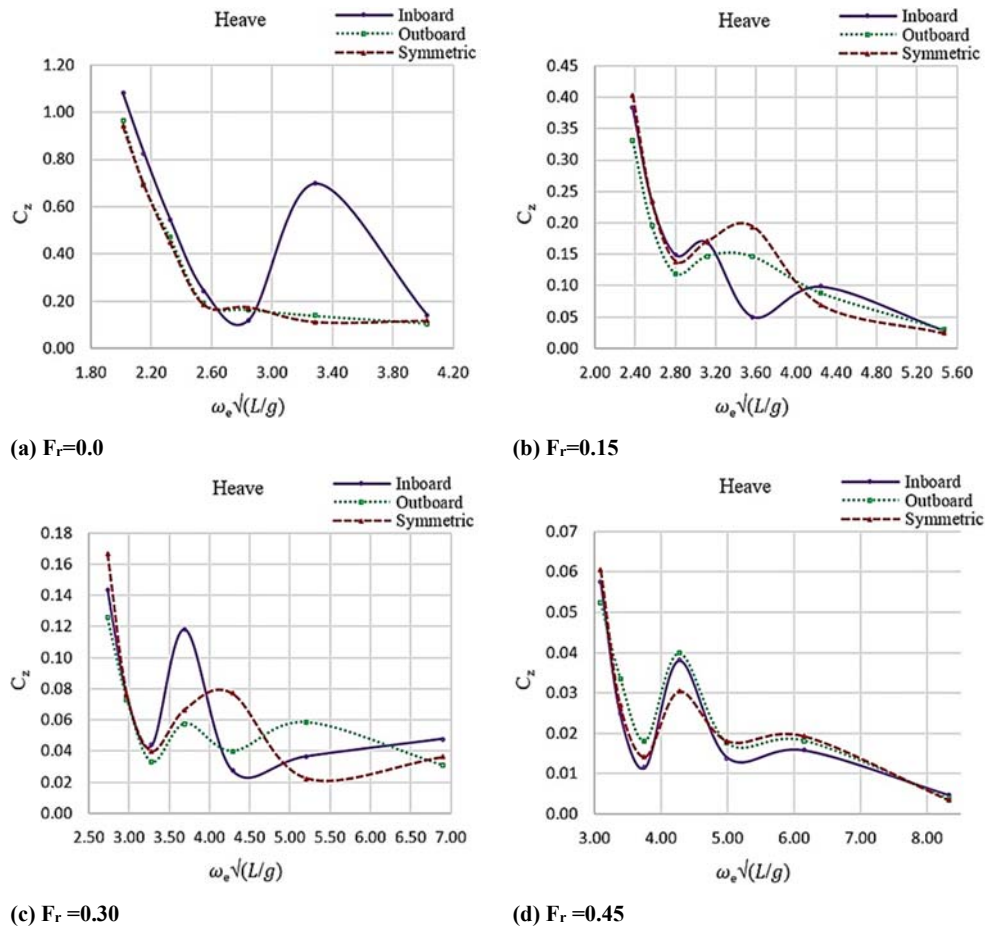

(a) F_r=0.0

(b) F_r=0.15

(c) F_r =0.30

(d) F_r =0.45

Fig. 7. Comparison of Heave RAO of three side hull form of a trimaran model at wave amplitude = 35 mm and head wave.

(a) F_r=0.0

(b) F_r=0.15

(c) F_r =0.30

(d) F_r =0.45

Fig. 8 Comparison of Heave RAO of three side hull form of a trimaran model at wave amplitude = 35 mm and head wave.

A dynamic amplification of the heave motion response, possibly due to entrapment of (standing) waves, leads to the disturbance between main and side hulls. Moreover, the interactions between the heave motion responses with pitch motion have resulted in the frequent appearance of kinks in a coupled form. Some of these kinks are a direct manifestation of the resonance effects on the model. This is because the kinks' frequencies are similar to the resonant frequencies of the model.

Figure 8 illustrates the heave RAO of the individual side hull form at the wave amplitude of 35 mm. As depicted in this figure, the heave responses were linear versus wave frequencies for the non-dimensional encounter frequencies ranging from 2.01 to 2.54 at the zero speed model (F_r=0), 2.4 to 2.8 at the model speed of 0.58 (F_r=0.15), 2.73 to 3.28 at the model speed of 1.155 m/s (F_r=0.3), and 3.08 to 3.57 at the model speed of 1.73 m/s (F_r=0.45). In the remaining non-dimensional encounter frequencies, the responses showed a nonlinear behaviour. They were also associated with certain kinks. It is perceived that at zero speed condition (Fig. 8(a)), the trend of heave responses for outboard and symmetric side hull form were generally similar to physical trends and magnitudes. The trend of the plot for the inboard was different because of the presence of a big kink in the responses at a non-dimensional encounter wave frequency of 3.28. There was an unequivocal difference between the magnitudes of the kinks of the outboard side hull form which had the highest responses at the Froude number of 0.30. As depicted in Fig. 8(d), the physical trend of the results of the experiment was the same in all the three different side hulls. At this speed, the symmetric side hulls had the lowest kink magnitude at a non-dimensional encounter wave frequency of 4.26.

Briefly, in the heave motion, for a wave height of 25 mm, the inboard side hull did not record any kink at the zero speed and performed better than the other model. Moving from zero speed up to 0.58 m/s, the symmetric form gave lower heave responses for all the non-dimensional encounter frequencies and performed better than the outboard and inboard side hull form. It could be observed that in a wave height of 35mm at zero speed, the symmetric and outboard side hull performed generally similarly and better than the inboard. Moving from zero speed to 0.58, 1.155, and 1.73 m/s, inboard, outboard, and symmetric had a better performance, respectively.

(a) F_r=0.0

(b) F_r=0.15

(c) F_r =0.30

(d) F_r =0.45
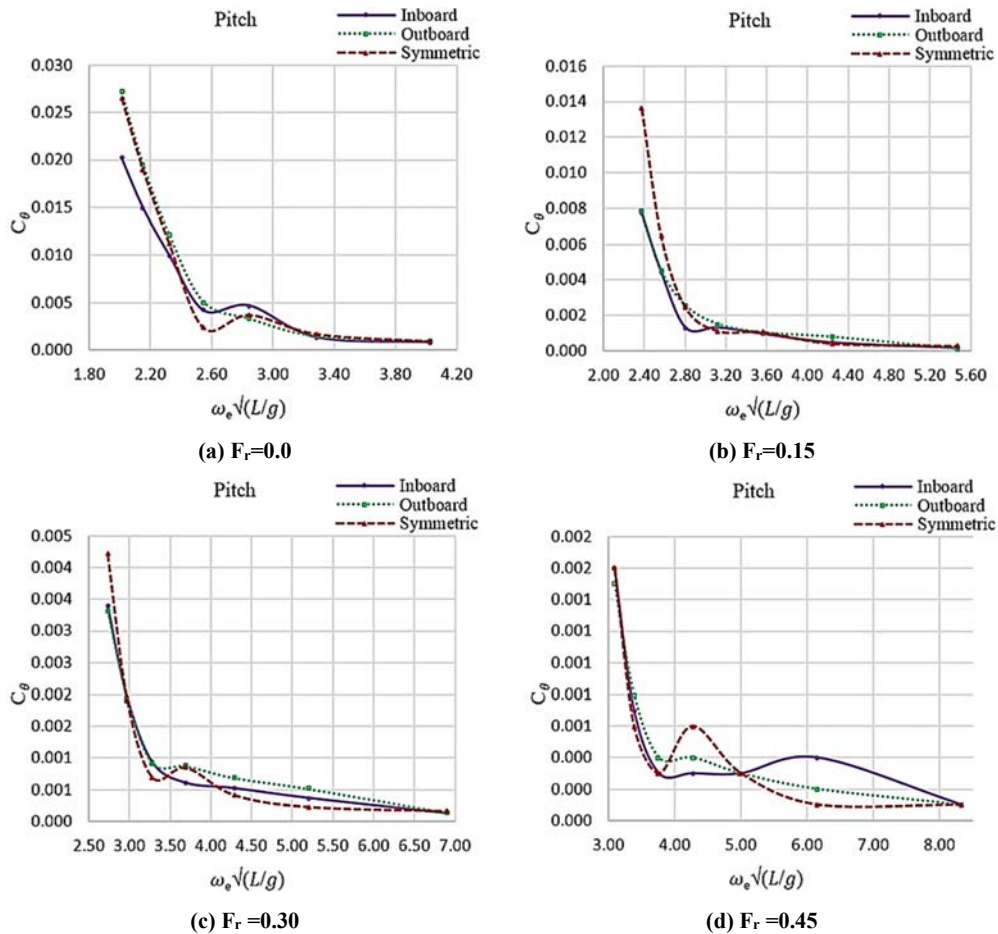
Fig. 9. Comparison of Pitch RAO of three side hull form of a trimaran model at wave amplitude = 25 mm and head wave.

The comparison of the pitch motion responses of the three models is depicted in Figs. 9 and 10. Figure 9 shows the comparison of pitch RAO at the wave amplitude of 25 mm. As depicted in Fig. 9 (a, b, and c), at the model speeds of 0.0, 0.58, and 1.155 m/s (Froude numbers of 0.0, 0.15, 0.3), the pitch motions initially sharply decreased versus the non-dimensional encounter frequency until the non-dimensional encounter frequencies of 2.54, 2.8, 3.28, and 3.75 at the four speeds, respectively. However, for greater wave frequencies, the responses decreased slowly as the wave frequency increased. Furthermore, the magnitudes of the responses decreased with the increase in the model speeds. As depicted in Fig. 9 (a, b, and c), the physical trend of pitch motion results was relatively the same in the three side hull forms. As depicted in Fig. 9(d), at the model test speed of 1.73 m/s (F_r=0.45), the plots contained two small kinks in the responses at higher frequencies for the individual outriggers form. In this wave amplitude, the outboard side hull did not record any kink and performed better than the other forms. Figure 10 displays the comparison of pitch RAO at the wave amplitude of 35 mm. As depicted in this

figure, the trend of the plot was mostly linear for the non-dimensional encounter frequency ranging from 2.01 to 2.54 at the zero speed model (F_r=0.0), 2.4 to 2.8 at the model speed of 0.58 (F_r=0.15), 2.73 to 2.8 at the model speed of 1.155 m/s (F_r=0.3), and 3.08 to 3.57 at the model speed of 1.73 m/s (F_r=0.45). The responses then revealed a nonlinear behaviour at the remaining frequencies. Furthermore, the magnitudes of the responses decreased with the increase in the model speeds. The trend of the RAO plots for the pitch responses depicted in Fig. 10(a) seemed to follow the similar patterns in symmetric and outboard outriggers. Nevertheless, at the model speeds of 0.58, 1.155, and 1.73 m/s (Froude numbers of 0.15, 0.30, and 0.45), the plots of the symmetric and inboard outriggers comprised some kinks with low magnitudes in the responses. Outboard side hull pitch responses steadily declined versus the non-dimensional encounter frequency, and no kinks were recorded in the responses. The comparison of the RAO among the three configurations implied that the trimaran model with outboard side hulls outperforms better than the other cases.
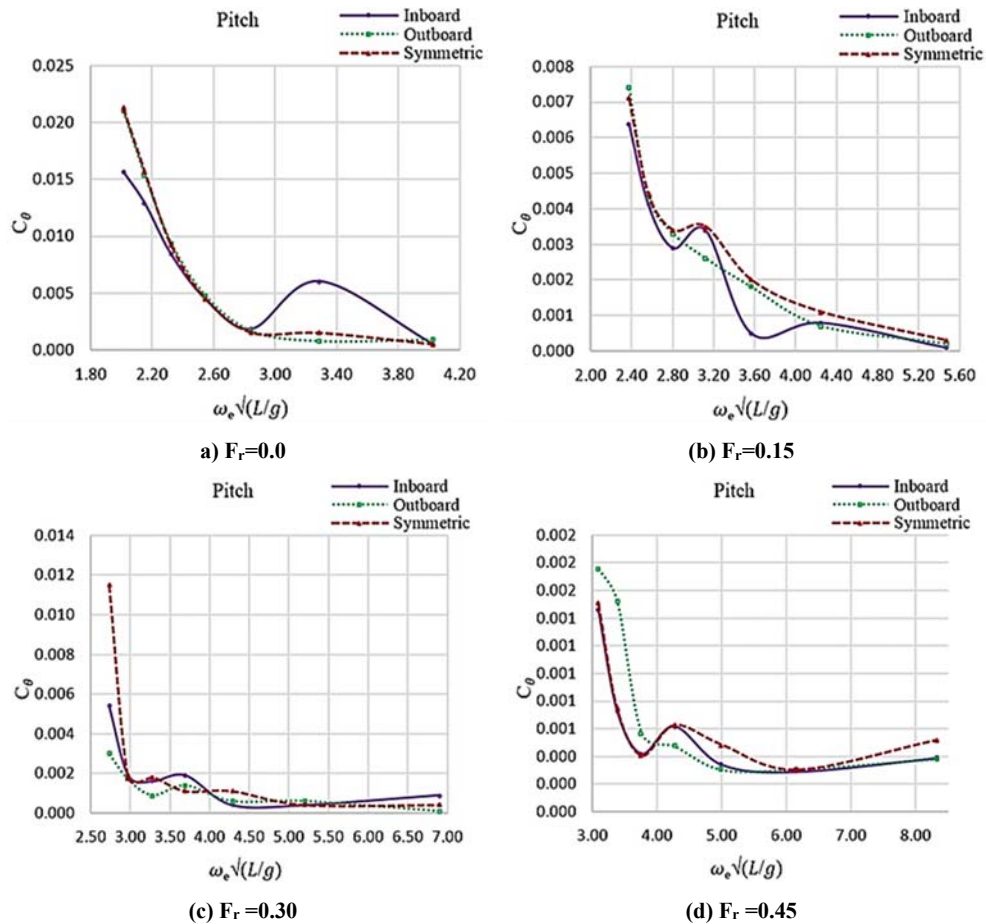
Fig. 10. Comparison of Pitch RAO of three side hull form of a trimaran model at wave amplitude = 35 mm and head wave.

In summary, the pitch motions responses showed that in a wave height of 25 mm at the speed of 0.0, 0.58, and 1.73 m/s, the outboard side hull performed better than the other forms. At the speed of 1.155 m/s, the inboard had a better performance. In a wave height of 35 mm for all the regions of speed, the outboard side hull performed better than the other forms.

Figures 11 and 12 demonstrate the effect of side hulls symmetry on the added resistance coefficient of trimaran for two different values of the wave amplitudes of 25 and 35 mm. As depicted in Fig. 11, the results were almost similar in physical trend for the three individual outriggers and the added resistance coefficient decreased with the increase in frequencies. At the model speed of 0.58 m/s (F_r=0.15), it could be said that the model with symmetric side hulls performed slightly better than that with the outboard. At the model speeds of 1.155 and 1.73 m/s (Froude numbers of 0.30, 0.45), the outboard side hull had the lowest value and a better performance than the other forms.

The comparison of the added resistance coefficient of individual side hull form at the wave amplitude of 35 mm is depicted in Fig. 12. It indicates that the variation of the added resistance of the three forms

were complex and their performances varied in the three model speeds. It has been established that the outboard concept slightly outperformed the other forms in terms of having lower magnitudes of added resistance at higher non-dimensional encounter wave frequencies. For trimaran configuration, the wave interaction between the centre hull and the outriggers has an important effect on interference resistance. The side hull forms, including inboard, outboard, and symmetric hulls, affected the interference drag. The high degree of inner side curvature amplified the wave interaction between the main hull and side hulls, leading to an increase in the interference drag. On the contrary, when the inner side is flat along the entire face of the outrigger, the interference resistance becomes weaker.

Briefly, for the added resistance in a wave height of 25 mm at the model speed of 0.58 m/s, the symmetric side hulls performed slightly better. Moving from 0.58 m/s to model speeds of 1.155 and 1.73 m/s, the outboard side hull had a better performance than the other forms. In the wave height of 35 mm for all the regions of speed, at low encounter wave frequencies, the symmetric and at high encounter wave frequencies, the outboard performed better that the other side hull forms.
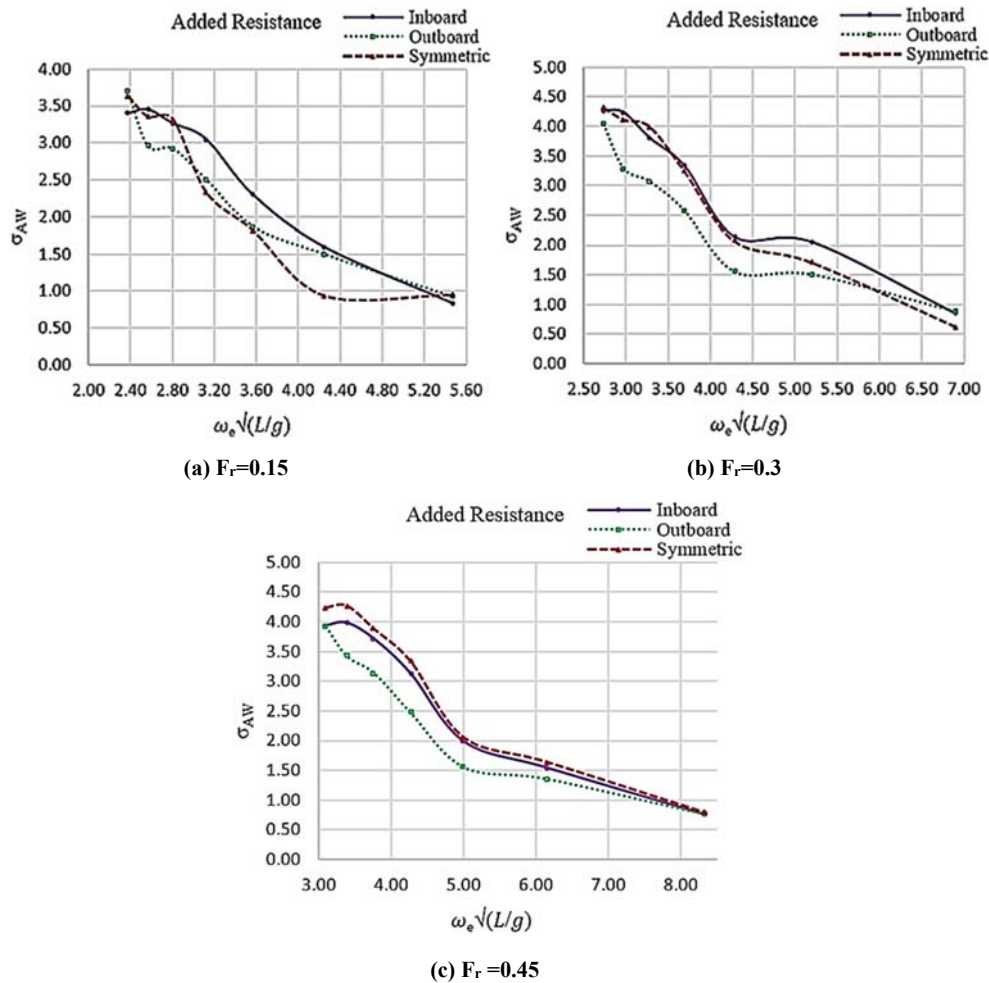
(a) F_r=0.15

(b) F_r=0.3

(c) F_r =0.45

Fig. 11. Comparison of added resistance of three side hull form of a trimaran model at wave amplitude = 25 mm and head wave.

4. CONCLUSION

The obtained model test results illustrated the impact of the outriggers geometry on the resultant resistance force and the trimaran heave and pitch motion responses. The conclusions in the current work were as follows:

- The interactions between the pitch and heave motion responses as well as the main and side hull interference (standing wave) phenomenon lead to the frequent appearance of kinks (local minimum and maximum) in the responses of wave-induced motions. Some of these kinks are a direct manifestation of the resonance effects on the model. This is because the kinks' frequencies are similar to the resonant frequencies of the model. The effects of these kinks could be adverse on the performance of the vessel.

- It seemed that the heave and pitch responses were sensitive to the model speed and the magnitudes of the responses decreased with the increase in the model speeds.

- According to the comparison between the heave motion responses, it was established that symmetric concepts performed better than the other concepts at the wave amplitude of 0.25m at all the speeds. Further comparison of the models performance at the wave amplitude of 0.35m indicated that symmetric concept performed better than outboard and inboard, particularly at the model speeds of 0.58 and 1.155 m/s (Froude numbers of 0.15, 0.30), in which outboard had better performance with modest kink magnitudes.

- Based on the comparison between the pitch motion responses, the outboard side hull responses steadily declined, did not show any kinks, and outperformed the other forms.

- It has been established that the outboard concept functioned slightly better than the other forms in terms of having lower magnitudes of the added resistance. Regarding trimaran configuration, the wave interaction between the central hull and the

(a) F$_r$=0.15

(b) F$_r$=0.3

(c) F$_r$ =0.45
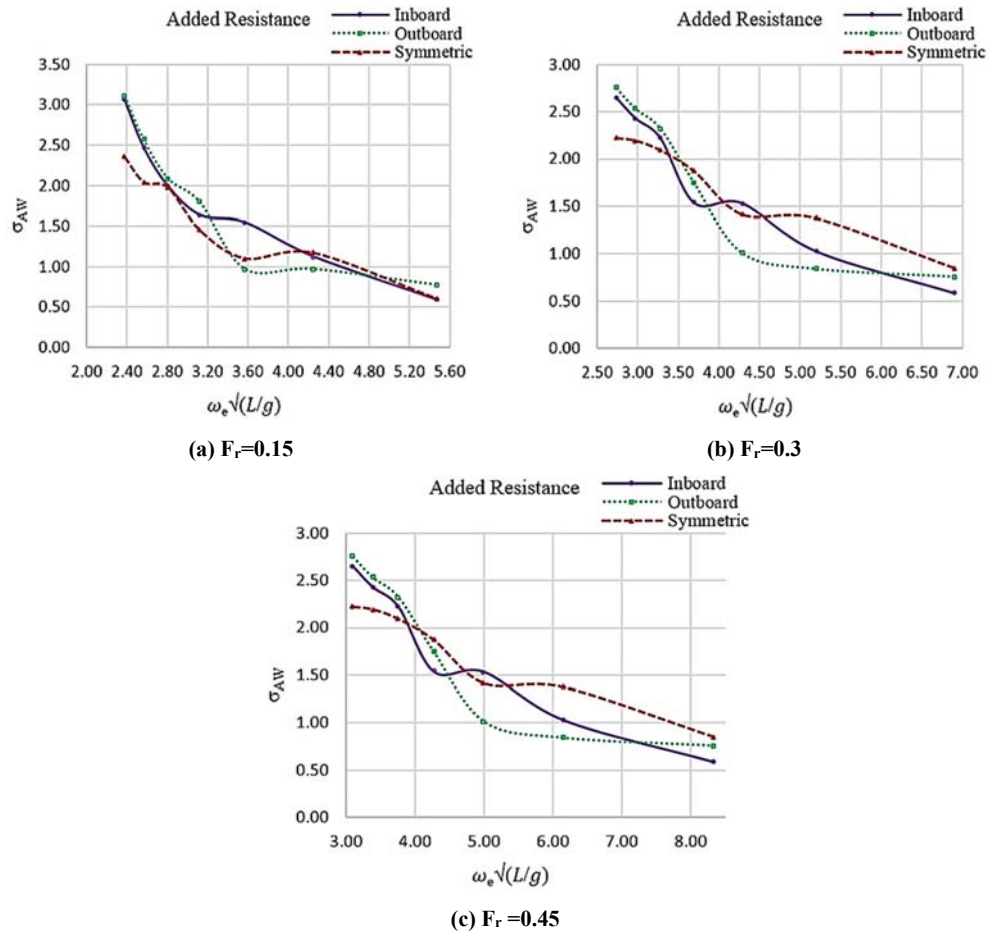
Fig. 12. Comparison of added resistance of three side hull form of a trimaran model at wave amplitude = 35 mm and head wave.

outriggers is of an important effect on the interference resistance. The high degree of inner side curvature amplified the wave interaction between the main hull and side hulls, leading to an increase in the interference drag. On the contrary, once the inner side was flat along the entire face of the outrigger, the interference resistance became weaker.

REFERENCES

Akbari Vakilabadi, K., M. R. Khedmati and M. Seif (2016). Experimental Study on Heave and Pitch Motion Characteristics of a Wave-Piercing Trimaran, *Transactions of FAMENA* XXXVIII-3, 13-26.

Atlar, M., D. B. Seren and J. Validakis (1985). The Effect of Tilt and Interference on the hydrodynamic Coefficients of SWATH-Type Sections, SWATH Ships and Advanced Multi-Hulled Vessels. London, UK, 17th -19th April 1985.

Armstrong, T. (2006). On the performance of a large high-speed trimaran. *Australian Journal of Mechanical Engineering* 3(2), 123–131.

Chen, Z., H. Gui, P. Dong and C. Yu (2019). Numerical and experimental analysis of hydroelastic responses of a high-speed trimaran in oblique irregular waves. *International Journal of Naval Architecture and Ocean Engineering* 11(1), 409–421.

Davis, M. R. and D. S. Holloway (2007). A comparison of the motions of trimarans, catamarans and monohulls. *Australian Journal of Mechanical Engineering* 4(2), 183–195.

Deng, R., F. Luo, T. Wu, S. Chen and Y. Li (2019). Time-domain numerical research of the hydrodynamic characteristics of a trimaran in calm water and regular waves. *Ocean Engineering* 194, 106669.

Deng, Q.，X. Mao and M. Wu (2016). Effect of principal dimensions on seakeeping and wave loads of Trimarans, *Chinese Journal of Ship Research* 11(6), 8-14.

Fang, M. C. and G. Y. Too (2006). The Effect of Side Hull Arrangements on the Motions of the Trimaran Ship in Waves. *Naval Engineers Journal* 118(1), 27–37.

Gong, J., S. Yan, Q. Ma and Y. Li (2020). Added resistance and seakeeping performance of trimarans in oblique waves. *Ocean Engineering* 216, 107721.

Hebblewhite, K., P. K. Sahoo and L. J. Doctors (2007). A case study: theoretical and experimental analysis of motion characteristics of a trimaran hull form. *Ships and Offshore Structures* 2(2), 149–156.

ITTC Recommended Procedures and Guidelines, (2017). *Global Loads Seakeeping Procedure*. ITTC 7.5-02-07-02.6, Technical Report, ITTC.

Jiao, J., C. Chen and H. Ren (2019). A comprehensive study on ship motion and load responses in short-crested irregular waves. *International Journal of Naval Architecture and Ocean Engineering* 11(1), 364–379.

Jiang, Y., H. Sun, J. Zou, A. Hu and J. Yang (2016). Analysis of tunnel hydrodynamic characteristics for planing trimaran by model tests and numerical simulations. *Ocean Engineering* 113, 101–110.

Li, A. and Y. Li (2019). Numerical and Experimental Study on Seakeeping Performance of a High-Speed Trimaran with T-foil in Head Waves. *Polish Maritime Research* 26(3), 65–77.

Nowruzi, L., H. Enshaei, J. Lavroff, S. S. Kianejad and M. R. Davis (2020a). CFD Simulation of Motion Response of a Trimaran in Regular Head Waves. *International Journal of Maritime Engineering* 162(A1).

Nowruzi, L., H. Enshaei, J. Lavroff and M. R. Davis (2020b). Parametric study of seakeeping of a trimaran in regular oblique waves. *Ships and Offshore Structures* 15(sup1), S98–S109.

Poundra, G. A. P., I. K. A. P. Utama, D. Hardianto and B. Suwasono (2017). Optimizing Trimaran Yacht Hull Configuration Based on Resistance and Seakeeping Criteria. *Procedia Engineering* 194, 112–119.

Pavkov, M. and M. Morabito (2014). Experimental Investigation of Trimaran Models in Shallow Water. *Journal of Ship Production and Design* 30(2), 66–78.

Pérez Fernández, R. (2012). Seakeeping in the navigation example in trimaran ship. *International Journal for Traffic and Transport Engineering* 2(3), 221–235.

Tang, H., H. Ren, P. Yu and B. Tian (2020a). Experimental investigation of seakeeping performance and load response of trimaran in small heeling condition. *Applied Ocean Research* 101, 102275.

Tang, H., X. Zhang, H. Ren and P. Yu (2020b). Numerical study of trimaran motion and wave load prediction based on time-domain Rankine-Green matching method. *Ocean Engineering* 214, 107605.

Wang, S. M., S. Ma and W. Y. Duan (2018). Seakeeping optimization of trimaran outrigger layout based on NSGA-II. *Applied Ocean Research* 78, 110–122.

Wu, C., D. Zhou, L. Gao and Q. Miao (2011). CFD computation of ship motions and added resistance for a high speed trimaran in regular head waves. *International Journal of Naval Architecture and Ocean Engineering* 3(1), 105–110.